Theoretical and Experimental Studies on Vibration Resistance of Composite Plates with Damping Coating

Yichen Deng[1,2], Yezhuang Jin[1,2,*], Yao Yang[2], Bocheng Dong[2] and Zelin Li[2], Hui Li[2]

[1]*College of Aerospace Engineering, Shenyang Aerospace University, Shenyang 110136*

[2]*School of Mechanical Engineering & Automation, Northeastern University, Shenyang 110819*

Abstract: This study performs both theoretical and experimental studies on the vibration resistance of composite plates with damping coating subjected to impulse excitation load. A dynamic model is first proposed and the key differential equations are derived to solve the natural frequencies, time-domain vibration response, and dynamic stiffness at any vibration response point regarding the excitation point of such a coated structure. Then, a dynamic experiment system of two plate specimens with and without DC knocked by a hammer excitation is set up. The measured data indicates that the proposed dynamic model is trustworthy for predicting natural frequencies and dynamic stiffness results. Furthermore, based on the calculated dynamic stiffness data associated with the first four modes, the anti-vibration contribution of DC is quantitatively evaluated. It can be found that the coating can indeed improve the vibration resistance of the structure by up to 74.7%. In addition, the vibration suppression effect of DC is found to be closely related to the mode order of such a structure as well as the selected boundary condition.

Keywords: Damping coating, Composite plate, Vibration resistance, Dynamic model.

1. INTRODUCTION

Composite plates (CPs) are being widely utilized in various engineering fields due to their lightweight and high stiffness property [1-3]. However, many vibration damages and fatigue problems often occur in these structures because many of them work in harsh dynamic conditions [4-6]. Damping coating (DC) is one of the advanced surfacing materials exhibiting an extensive application prospect since it has the advantages of low cost, high vibration reduction, and strong corrosion resistance, etc [7, 8]. The publicized literature [9, 10] has proven its excellent performance compared to conventional coating materials. However, the related investigations into the DC-CPs are in their infancy, including the modeling technique, experiment approach, optimization design, etc.

In the past few decades, lots of research effort has been devoted to the vibration suppression performance of various composite plates with different methods. For example, Zhang *et al*. [11] conducted a series of experiments on a composite elastomeric isolator to evaluate its energy dissipation capacity. Also, the deformation assumptions used in the theoretical method are validated via finite element data. The vibration responses of fiber-steered laminated plates were predicted by Akbarzadeh *et al*. [12] based on third-order shear deformation theory, the hybrid Fourier-Galerkin approach, and the numerical integration technique. He *et al*. [13] proposed an analytical model to analyze the vibration absorption capacity of fiber-reinforced laminated plates with mass-spring-damper subsystems. The stopband behavior of such structures was further evaluated by performing a frequency response analysis. Based on the first-order shear deformation theory and von Karman nonlinear transformation theory, Shivakumar *et al*. [14] established a finite element (FE) model with eight-node isoparametric serendipity elements to predict the active damping characteristics of the composite plates with the patches of active fiber composites. Zu *et al*. [15] proposed a new nonlinear vibration model of a thin composite sheet in a thermal environment, in which the complex modulus approach, the power function, and the Ritz methods were adopted to introduce the nonlinear thermal and amplitude fitting coefficients into this model. Additionally, the measured natural frequencies, damping ratios, and vibration responses were employed to prove the good prediction capability of such a model. The damped free vibration properties of woven glass fiber-reinforced epoxy composite plates were measured and simulated by Navaneeth *et al*. [16]. They pointed out that the frequency response displayed an upward trend as the number of layers of the composite plate increased.

With the advantages of the DC, it is often utilized as surface improvement technology to achieve a better anti-vibration capability of different coated structures. Several articles have reported the progress in the structural dynamics of composite plates with DC. For

*Address correspondence to this author at the College of Aerospace Engineering, Shenyang Aerospace University, Shenyang 110136;
Tel: + 861062787863; E-mail: jyz8133@163.com

instance, based on experimental data, Mohotti *et al*. [17] identified the damping behavior of composite aluminum plates covered with polyurea damping coating subjected to low-velocity impact loadings. Moreover, they established a FE model by LS-DYNA to quantify the energy absorption performance of such a damping coating with different configurations. By using a FE plate model, Kulhavy *et al*. [18] evaluated the additional damping behaviours of fiber-reinforced plates coated with viscoelastic neoprene and thin rubber material. They also performed experimental tests to validate the FE model as well as to find the nonlinear damping phenomenon. An improved component mode mistuning model is proposed by Xu *et al*. [19] to identify the damping properties of the hard and viscoelastic coated blisks. Gao *et al*. [20] also conducts numerical studies on blisks with tuned and mistuning coatings to evaluate the influence of intentional mistuning hard coatings on vibration characteristics of the structure. Wang and his coauthors [21, 22] investigated the frequency responses, natural frequencies, mode shapes, and damping loss factors of a corrugated sandwich panel with polyurea coating, in which a mixed experimental and numerical approach was employed to quantify the benefit of coating material in the face sheets on the passive vibration attenuation of such a coated structure. A long coated damping structure with entangled metallic wire material is proposed by Zi *et al*. [23] to investigate the effects of coating thickness, coating length and the temperature on vibration attenuation.

The aforementioned literature review reveals that there are limited publications concerning the vibration resistance of the DC-CP structures. In particular, no one has utilized the dynamic stiffness results to evaluate the anti-vibration performance of coated composite structures based on an analytical model developed. To cover this knowledge gap, by taking a fiber-reinforced composite plate with DC as a research object, the corresponding vibration suppression analysis work is done in this study. In Section 2, a dynamic model subjected to a pulse excitation load is proposed, and then the solution expression of dynamic stiffness is derived. Moreover, some detailed tests are undertaken to validate the model as well as to investigate the anti-vibration performance of coated plate specimens with DC in Section 3. The theoretical modelling and experimental techniques used in this paper can provide a meaningful reference for studying the vibration resistance of composite structures with an advanced coating material.

2. THEORETICAL WORK

2.1. Model Description

A dynamic model of the DC-CP structure subjected to a pulse excitation load is illustrated in Figure **1**, where an *o-xyz* coordinate system is established at the mid-plane of the uncoated plate, with '1', '2', and '3' denoting three principal fiber axes, respectively, and θ being the angle between the 1- and *x*-axis. The overall length, width, and the total number of layers of fiber-reinforced plate are represented by *a*, *b*, and *n*, respectively. The DC is assumed to be sprayed evenly

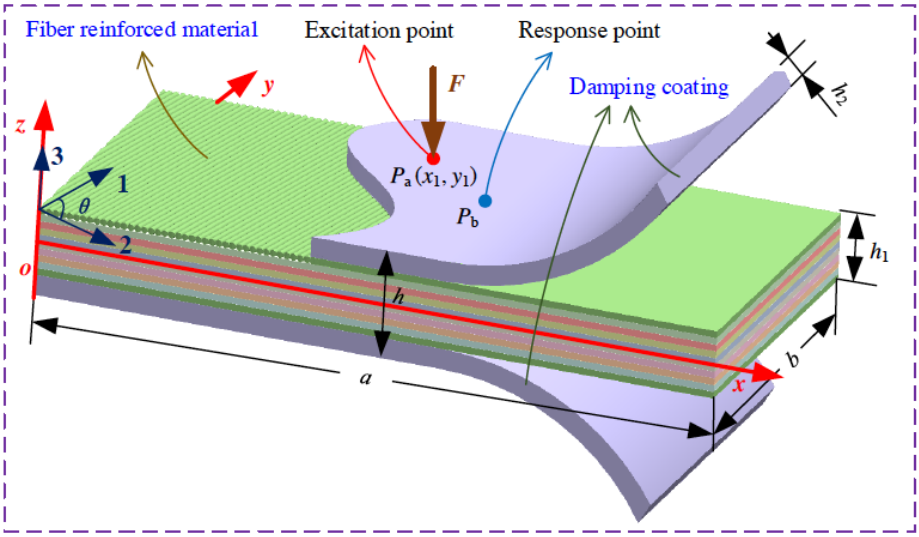

Figure 1: A dynamic model of the DC-CP structure subjected to a pulse excitation load.

on both sides of the plate. The thickness values of the coated and uncoated plate, and the DC are assumed to be h, h_1, and h_2, respectively. The impulsive excitation point is supposed to be at P_a (x_1, y_1), and the dynamic response point is at P_b (x_2, y_2).

2.2. Displacement Field Assumption

The studied plate with DC is assumed as a symmetric laminated structure. Based on the first-order shear deformation theory [24], the displacements field of this structure can be expressed as:

$$\begin{aligned} u(x,y,z,t) &= u_0(x,y,t)+z\varphi(x,y,t) \\ v(x,y,z,t) &= v_0(x,y,t)+z\psi(x,y,t) \\ w(x,y,z,t) &= w_0(x,y,t) \end{aligned} \tag{1}$$

where u, v, w are the displacements of the DC-CP structure in the x, y, and z directions, u_0, v_0, and w_0 represent the related displacements at the mid-plane, φ and ψ are the rotations of transverse normal in the xoz and yoz planes, respectively, and t is the time variable.

Assume that there is only a weak coupling effect between the bending motion and the stretching motion of the DC-CP structure. Thus, u_0 and v_0 can be neglected [25]. As a result, the corresponding stress-strain relationships are expressed as:

$$\begin{cases} \varepsilon_x = \dfrac{\partial u}{\partial x} = z\varphi_{,x}; \varepsilon_y = \dfrac{\partial v}{\partial y} = z\psi_{,y}; \varepsilon_z = \dfrac{\partial w}{\partial z} = 0 \\ \gamma_{xy} = \dfrac{\partial u}{\partial y} + \dfrac{\partial v}{\partial x} = z\left(\varphi_{,y} + \psi_{,x}\right) \\ \gamma_{yz} = k_x \cdot \left(\dfrac{\partial w}{\partial y} + \dfrac{\partial v}{\partial z}\right) = k_x \cdot \left(\psi + w_{,y}\right) \\ \gamma_{xz} = k_x \cdot \left(\dfrac{\partial w}{\partial x} + \dfrac{\partial u}{\partial z}\right) = k_x \cdot \left(\varphi + w_{,x}\right) \end{cases} \tag{2}$$

where ε_x, ε_y, γ_{xy}, γ_{xz}, γ_{yz} are the normal and shear strains in the x, y, and z directions, respectively, and $k_x = \pi^2/12$ is a shear correction factor.

Supposing the DC-CP structure is constrained by a fully constrained boundary at the four edges, the displacement field functions need to meet the following conditions:

$$\begin{aligned} &w(0,y,t) = w(a,y,t) = w(x,0,t) = w(x,b,t) = 0 \\ &\frac{\partial w}{\partial x}(0,y,t) = \frac{\partial w}{\partial x}(a,y,t) = \frac{\partial w}{\partial y}(x,0,t) = \frac{\partial w}{\partial y}(x,b,t) = 0 \\ &\varphi(0,y,t) = \varphi(a,y,t) = \psi(x,0,t) = \psi(x,b,t) = 0 \end{aligned} \tag{3}$$

According to the Ritz method [26], the displacement relation can be formulated as:

$$\begin{aligned} \varphi &= \sum_{m=1}^{M}\sum_{n=1}^{N} \alpha_{mn} P_m(\xi) P_n(\eta) \sin(\omega t) \\ \psi &= \sum_{m=1}^{M}\sum_{n=1}^{N} \beta_{mn} P_m(\xi) P_n(\eta) \sin(\omega t) \\ w_0 &= \sum_{m=1}^{M}\sum_{n=1}^{N} \gamma_{mn} P_m(\xi) P_n(\eta) \sin(\omega t) \end{aligned} \tag{4}$$

where α_{mn}, β_{mn}, and γ_{mn} are the undetermined coefficients, $P_m(\xi)$ and $P_n(\eta)$ are the vibration mode functions of the DC-CP structure, ω represents the natural circular frequency, and M and N are the numbers of truncated terms by the Rayleigh-Ritz method. As reported by our previous study [27], $M = N = 8$ is adopted to ensure the calculating precision.

Next, based on the Schmidt Orthogonalization principle, the following vibration mode functions are obtained to satisfy boundary conditions:

$$\begin{aligned} P_1(\xi) = \chi(\xi),\ P_1(\eta) = \kappa(\eta) \\ P_2(\zeta) = (\zeta - B_2) P_1(\zeta)\zeta \\ P_k(\zeta) = (\zeta - B_k) P_{k-1}(\zeta) - C_k P_{k-2}(\zeta) \\ \zeta = \xi, \eta, \quad k > 2 \end{aligned} \tag{5}$$

where B_k and C_k are the coefficient functions given by Eq. (6):

$$\begin{aligned} B_k &= \frac{\int_0^1 W(\zeta)\left[P_{k-1}(\zeta)\right]^2 \zeta d\zeta}{\int_0^1 W(\zeta)\left[P_{k-1}(\zeta)\right]^2 d\zeta} \\ C_k &= \frac{\int_0^1 W(\zeta) P_{k-1}(\zeta) P_{k-2}(\zeta)\zeta d\zeta}{\int_0^1 W(\zeta)\left[P_{k-2}(\zeta)\right]^2 d\zeta}, \zeta = \xi, \eta \end{aligned} \tag{6}$$

where $W(\zeta)$ is the weight function, and $\chi(\xi)$ and $\kappa(\eta)$ are the polynomial coefficients. Since the structure is constrained with four sides, the expressions of $\chi(\xi)$ and $\kappa(\eta)$ can be determined as:

$$\begin{aligned} \chi(\xi) = \xi^2(1-\xi)^2, \quad \kappa(\eta) = \eta^2(1-\eta)^2 \\ \xi = x/a, \quad \eta = y/b \end{aligned} \tag{7}$$

2.3. Solution of Natural Characteristics

Assuming that the constitutive relationship expression of the DC-CP structure is as follows:

$$\begin{Bmatrix}\sigma_x\\ \sigma_y\\ \tau_{yz}\\ \tau_{xz}\\ \tau_{xy}\end{Bmatrix}=\begin{bmatrix} Q_{11} & Q_{12} & & & & \\ Q_{12} & Q_{22} & & & & \\ & & Q_{44} & & & \\ & & & Q_{55} & & \\ & & & & Q_{66} & \end{bmatrix}\begin{Bmatrix}\varepsilon_x\\ \varepsilon_y\\ \gamma_{yz}\\ \gamma_{xz}\\ \gamma_{xy}\end{Bmatrix} \tag{8}$$

where for the coating material, $Q_{11}=Q_{22}=\frac{E_{\mathrm{p}}^*}{1-\mu_{\mathrm{p}}}, Q_{12}=\frac{\mu_{\mathrm{p}}E_{\mathrm{p}}^*}{1-\mu_{\mathrm{p}}}, Q_{44}=Q_{55}=Q_{66}=\frac{E_{\mathrm{p}}^*}{2(1+\mu_{\mathrm{p}})}$ re presents the stiffness coefficients, with E_{p}^* being the complex elastic modulus with the expression of $E_{\mathrm{p}}^*=E_{\mathrm{p}}\left(1+\mathrm{i}\eta_{\mathrm{p}}\right)$. Here, E_{p} and η_{p} represent the traditional elastic modulus and loss factor of coating material.

For fiber reinforced material, suppose that the complex elastic moduli E_{f1}^*, E_{f2}^*, and complex shear moduli G_{f12}^*, G_{f13}^*, G_{f23}^* in different fiber directions can be defined as:

$$\begin{aligned}
&E_{\mathrm{f1}}^*=E_{\mathrm{f1}}\left(1+\mathrm{i}\eta_{\mathrm{f1}}\right);\\
&E_{\mathrm{f2}}^*=E_{\mathrm{f2}}\left(1+\mathrm{i}\eta_{\mathrm{f2}}\right);\\
&G_{\mathrm{f12}}^*=G_{\mathrm{f12}}\left(1+\mathrm{i}\eta_{\mathrm{f12}}\right);\\
&G_{\mathrm{f13}}^*=G_{\mathrm{f13}}\left(1+\mathrm{i}\eta_{\mathrm{f13}}\right);\\
&G_{\mathrm{f23}}^*=G_{\mathrm{f23}}\left(1+\mathrm{i}\eta_{\mathrm{f23}}\right)
\end{aligned} \tag{9}$$

where E_{f1} and E_{f2} are the traditional elastic moduli; G_{f12}, G_{f13}, and G_{f23} represent the traditional shear moduli; η_{f1}, η_{f2}, η_{f12}, η_{f13}, and η_{f23} denote the traditional loss factors in different fiber directions.

Then, the corresponding off-axis stress-strain relationship of the composite plate is stated as:

$$\begin{Bmatrix}\sigma_x\\ \sigma_y\\ \tau_{yz}\\ \tau_{xz}\\ \tau_{xy}\end{Bmatrix}^k=\Gamma\begin{bmatrix} Q_{11} & Q_{12} & 0 & 0 & 0\\ Q_{12} & Q_{22} & 0 & 0 & 0\\ 0 & 0 & Q_{44} & 0 & 0\\ 0 & 0 & 0 & Q_{55} & 0\\ 0 & 0 & 0 & 0 & Q_{66}\end{bmatrix}\Gamma^{\mathrm{T}}\begin{Bmatrix}\varepsilon_x\\ \varepsilon_y\\ \gamma_{yz}\\ \gamma_{xz}\\ \gamma_{xy}\end{Bmatrix}^k \tag{10}$$

where Γ is the coordinate transformation matrix with the following expression:

$$\Gamma=\begin{bmatrix} c^2 & s^2 & 0 & 0 & -2cs\\ s^2 & c^2 & 0 & 0 & 2cs\\ 0 & 0 & c & s & 0\\ 0 & 0 & -s & c & 0\\ cs & -cs & 0 & 0 & c^2-s^2\end{bmatrix} \tag{11}$$

where $c=\cos\theta_k$; $s=\sin\theta_k$; θ_k is the angle between the 1- and *x*-axis in the *k*-th layer.

In Eq. (10), Q_{ij} represents the reduced stiffness coefficients of fiber reinforced material with the following expressions:

$$\begin{aligned}
&Q_{11}=\frac{E_{\mathrm{f1}}^*}{1-\mu_{\mathrm{f1}}\mu_{\mathrm{f2}}}, Q_{12}=Q_{21}=\frac{\mu_{\mathrm{f1}}E_{\mathrm{f2}}^*}{1-\mu_{\mathrm{f1}}\mu_{\mathrm{f2}}}=\frac{\mu_{\mathrm{f2}}E_{\mathrm{f1}}^*}{1-\mu_{\mathrm{f1}}\mu_{\mathrm{f2}}}\\
&Q_{22}=\frac{E_{\mathrm{f2}}^*}{1-\mu_{\mathrm{f1}}\mu_{\mathrm{f2}}}, Q_{44}=G_{\mathrm{f23}}^*, Q_{55}=G_{\mathrm{f13}}^*, Q_{66}=G_{\mathrm{f12}}^*
\end{aligned} \tag{10}$$

where μ_{f1} and μ_{f2} are the Poisson's ratios of fiber layers.

The kinetic energies T_{p1}, T_{p2}, T_{f} and the strain energies U_{p1}, U_{p2}, U_{f} of the upper and lower layers of DC and fiber reinforced material, as shown in Figure **1** are, respectively, given by:

$$\begin{aligned}
T_{\mathrm{p1}}&=\frac{1}{2}\int_A\int_{h_1/2}^{h/2}\rho_{\mathrm{p}}\left[\left(\frac{\partial u}{\partial t}\right)^2+\left(\frac{\partial v}{\partial t}\right)^2+\left(\frac{\partial w}{\partial t}\right)^2\right]\mathrm{d}z\mathrm{d}A\\
T_{\mathrm{f}}&=\frac{1}{2}\int_A\int_{-h_1/2}^{h_1/2}\rho_{\mathrm{f}}\left[\left(\frac{\partial u}{\partial t}\right)^2+\left(\frac{\partial v}{\partial t}\right)^2+\left(\frac{\partial w}{\partial t}\right)^2\right]\mathrm{d}z\mathrm{d}A\\
T_{\mathrm{p2}}&=\frac{1}{2}\int_A\int_{-h/2}^{-h_1/2}\rho_{\mathrm{p}}\left[\left(\frac{\partial u}{\partial t}\right)^2+\left(\frac{\partial v}{\partial t}\right)^2+\left(\frac{\partial w}{\partial t}\right)^2\right]\mathrm{d}z\mathrm{d}A
\end{aligned} \tag{11}$$

$$\begin{aligned}
U_{\mathrm{p1}}&=\frac{1}{2}\int_A\int_{h_1/2}^{h/2}\left(\sigma_x\varepsilon_x+\sigma_y\varepsilon_y+\tau_{xy}\gamma_{xy}+\tau_{yz}\gamma_{yz}+\tau_{xz}\gamma_{xz}\right)\mathrm{d}z\mathrm{d}A\\
U_{\mathrm{f}}&=\frac{1}{2}\int_A\int_{-h_1/2}^{h_1/2}\left(\sigma_x\varepsilon_x+\sigma_y\varepsilon_y+\tau_{xy}\gamma_{xy}+\tau_{yz}\gamma_{yz}+\tau_{xz}\gamma_{xz}\right)\mathrm{d}z\mathrm{d}A\\
U_{\mathrm{p2}}&=\frac{1}{2}\int_A\int_{-h/2}^{-h_1/2}\left(\sigma_x\varepsilon_x+\sigma_y\varepsilon_y+\tau_{xy}\gamma_{xy}+\tau_{yz}\gamma_{yz}+\tau_{xz}\gamma_{xz}\right)\mathrm{d}z\mathrm{d}A
\end{aligned} \tag{12}$$

where ρ_{p} and ρ_{f} are the corresponding densities of polyuria coating and fiber layers, respectively.

Thus, the total kinetic energy *T* and strain energy *U* of the DC-CP structure can be obtained as:

$$T=T_{\mathrm{p1}}+T_{\mathrm{f}}+T_{\mathrm{p2}} \tag{13}$$

$$U = U_{\mathrm{p1}} + U_{\mathrm{f}} + U_{\mathrm{p2}} \tag{14}$$

By substituting Eq. (4) into Eqs. (15-16), the expressions of strain and kinetic energies can be obtained by the undetermined coefficients α_{mn}, β_{mn}, γ_{mn}. Furthermore, the corresponding maximum strain energy $U_{\max}$ and the maximum kinetic energy $T_{\max}$ can be expressed as:

$$\mathrm{U}_{\max} = \frac{1}{2}\boldsymbol{q}^{\mathrm{T}}\boldsymbol{K}\boldsymbol{q} \tag{15}$$

$$T_{\max} = \frac{1}{2}\omega^2\boldsymbol{q}^{\mathrm{T}}\boldsymbol{M}\boldsymbol{q} \tag{16}$$

where $\boldsymbol{K}$ and $\boldsymbol{M}$ are the stiffness and mass matrices, respectively, ω is the circular natural frequency of the structure studied, and $\boldsymbol{q}$ is the eigenvector $\boldsymbol{q} = \left(\alpha_{11},\alpha_{12},...,\alpha_{mn}\,|\beta_{11},\beta_{12},...,\beta_{mn}\,|\gamma_{11},\gamma_{12},...,\gamma_{mn}\right)^{\mathrm{T}}$.

The expression of Lagrange energy function L is defined as:

$$L = T_{\max} - U_{\max} \tag{17}$$

To solve the natural characteristics of the DC-CP structure based on the Rayleigh-Ritz method, one need to find the solution with a minimum value of L:

$$\left(\frac{\partial L}{\partial \alpha_{mn}}, \frac{\partial L}{\partial \beta_{mn}}, \frac{\partial L}{\partial \gamma_{mn}}\right) = 0 \quad m = 1,2,...,M; n = 1,2,...,N \tag{18}$$

Substituting Eqs. (17-19) into Eq. (20), one has

$$\left(\boldsymbol{K} - \omega^2\boldsymbol{M}\right)\boldsymbol{q} = 0 \tag{19}$$

To obtain the solutions of Eq. (21), the determinant of the coefficient matrix needs to be set as zero, *i.e.* $\left|\boldsymbol{K} - \omega^2\boldsymbol{M}\right| = 0$. Then, the natural frequency of the structure can be solved. Also, the corresponding mode shape can be calculated by substituting $\boldsymbol{q}$ into Eq. (4).

2.4. Solution of Dynamic Stiffness

Assuming that the expression of the impulse excitation load $F(x, y, t)$ and the structural vibration response $X(t)$ can be defined as:

$$F(x,y,t) = f(t)\,\delta(x - x_1)\delta(y - y_1)$$
$$f(t) = \begin{cases} f_0 \sin(\omega_f t) & , \quad 0 \le t \le t_1 \\ 0 & , \quad t > t_1 \end{cases} \tag{20}$$

$$X(t) = \sum_{m=1}^{\infty}\sum_{n=1}^{\infty} W_{mn}(x,y)T_{mn}(t) \tag{21}$$

where (x_1, y_1) is the coordinate of excitation point P_{a}, f_0 is the amplitude of excitation force, ω_{f} is the excitation frequency, t_1 is the lasting time of load, $W_{mn}(x,y)$ is the modal shape, and T_{mn} indicates the modal shape component of each order.

If the damping effect is considered, the vibration differential equation of the DC-CP structure can be written as:

$$\frac{\mathrm{d}^2 T_{mn}(t)}{\mathrm{d}t^2} + 2\zeta_r\omega\frac{\mathrm{d}T_{mn}}{\mathrm{d}t} + \left(\omega\right)^2 T_{mn}(t) = \frac{P_{mn}(t)}{M_{mn}} \tag{22}$$

where $P_{mn}(t)$ and M_{mn} are the generalized force and mass associated with the (m, n)-th mode shape, and ζ_r is the r-th modal damping ratio of the structure, which can be obtained from the experimental data.

By applying the Duhamel integral method to solve the differential equation when the initial condition value is zero, each of the modal shape component $T_{mn}(t)$ can be obtained as:

$$T_{mn}(t) = \frac{W_{mn}(x_1,y_1)}{\omega_{\mathrm{d}}M_{mn}}\int_0^t f(\tau)\mathrm{e}^{-\zeta_r\omega(t-\tau)}\sin\omega_{\mathrm{d}}(t-\tau)\mathrm{d}\tau \tag{23}$$

where $\omega_{\mathrm{d}} = \omega\sqrt{1-\zeta_r^2}$ is the natural circular frequency with consideration of damping.

After solving Eq. (25) by the numerical integration method of Simpson, and then the calculated result is substituted to Eq. (23). The time-domain vibration response of the structure subjected to impulse excitation load can be obtained by the mode superposition approach.

Furthermore, the dynamic stiffness expression at any vibration response point P_{b} regarding to the excitation point P_{a} of the DC-CP structure can be obtained as:

$$k_{ba}(\omega) = 1\Big/F\left[\frac{W_{mn}(x_1,y_1)}{\omega_{\mathrm{d}}M_{mn}}\int_0^t f(\tau)\sin\omega_{\mathrm{d}}(t-\tau)\mathrm{d}\tau\right] \tag{24}$$

where $F[y]$ denote to Fourier transform operation. Once $k_{ba}(\omega)$ is obtained, the dynamic stiffness results can be used to evaluate the vibration resistance of the studied structure system.

3. EXPERIMENTAL WORK

3.1. Experimental Specimen and System

Before the formal measurement is conducted, two plate specimens with the same geometric and material parameters are fabricated by a company, in which T300 carbon fiber/epoxy resin with the layout scheme of $[(0°/90°)_5/0°/(0°/90°)_5]$ is adopted and it include the 11 plies of unidirectional fiber prepregs. Then, one of the specimens is coated with polyurea material, a kind of DC, on the top and bottom surfaces via an SG9620 electric spray gun with a nozzle diameter of 1.8 mm, an air pressure of 0.6 Mpa, and a coating solidification time of about 1 min. Here, the polyurea material is produced by combining amine groups with isocyanate in a quick chemical reaction. The coating thickness is 0.6mm, with the additional weight being approximately 40% of the composite plate specimens. The other material and geometric properties of the specimens and the coating are: $G_{f12} = G_{f13} = G_{f23} = 4.6$Gpa, $E_{f1} = 120$Gpa, $E_{f2} = 7.9$Gpa, $\mu_{f1} = 0.30$, $\rho_f = 1780$kg/m^3, $E_p = 230$Mpa, $\mu_p = 0.40$, $\rho_p = 1020$kg/m^3.

A dynamic experiment system of the DC-CP specimens with a hammer excitation is set up, as shown in Figure **2**. The system is mainly composed of a DCB 086C01 modal hammer, a B&K 4517 lightweight acceleration sensor, an LMS data acquisition instrument with 16 channels, a mobile workstation. The tested specimens with and without DC are effectively clamped with its four sides via a clamping fixture. When the calibration experiments of the acceleration sensor and the hammer are finished, two specimens are knocked by the hammer at the same excitation point. Subsequently, the corresponding response signal and pulse excitation force are recorded by the data acquisition instrument. In this way, the dynamic stiffness curves can be measured via the LMS Test.Lab11A software. In the tests, $P_a(x_1, y_1) = (50$ mm, 50 mm) is set as the excitation point of each specimen, and $P_b(x_2, y_2) = (121, 100)$ is selected as the related response point, with the measured frequency range being within 10-1600 Hz.

Then, by adopting the half-power bandwidth technique, the damping ratios of the composite plate specimens without DC associated with the first four modes can be identified, which are 0.95, 0.80, 0.88, 0.93 %, respectively. Also, the related damping results of the coated specimen is measured, which are 1.07, 0.85, 0.95, and 1.04 %, respectively. By comparing these damping data of uncoated and coated specimens, it is clear that the DC material has a significant impact on the vibration suppression ability of this composite plate structure.

3.2. Model Validation and Evaluation of Vibration Resistance

To further quantitatively clarify the damping contribution of the coating material, the time history curves of the excitation force and the vibration response and dynamic stiffness results related to the

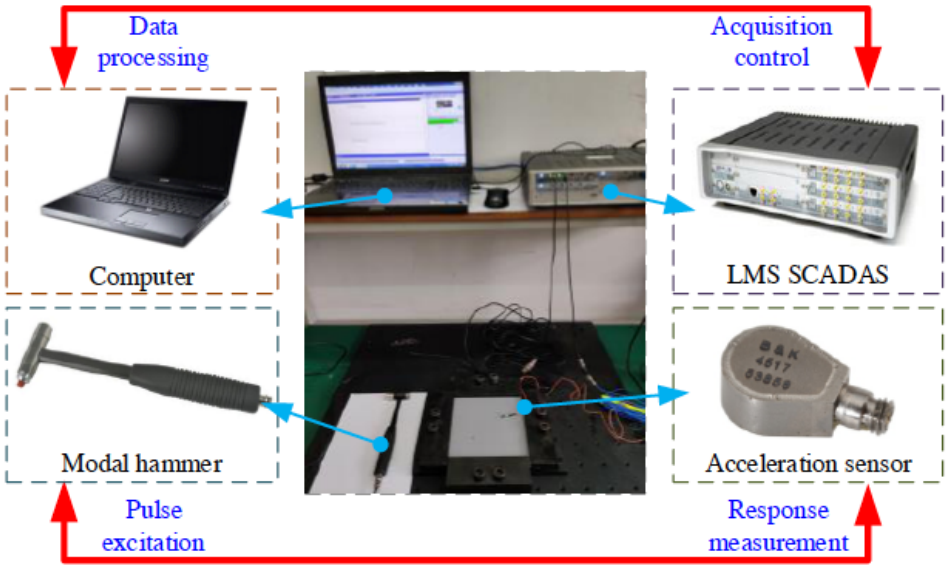

Figure 2: A dynamic experiment system of the DC-CP specimens with a hammer excitation.

first four modes of the coated and uncoated plate specimens obtained via experimental tests and theoretical calculations are compared in Figures **3** and **4**, respectively. One can find out that the calculated and measured data of the coated and uncoated specimens have a relatively good agreement. The maximum calculation error of natural frequency results with and without coating is R_{fre} = 4.2 %, and the corresponding error of dynamic stiffness results is R_k= 9.3%. Hence, it can be concluded that the proposed model is trustworthy for forecasting the dynamic stiffness curves of the composite plate structures, no matter whether the DC is considered or not. The above calculation error may come from: (1) a difference between the geometric and material parameters of coating adopted in the model and the actual specimen being tested. For example, the coating thickness is unequal for the coated specimen, but in the modelling process, only constant thickness is considered for DC; (2) a difference between the measured the simulated positions of excitation points or response points.

In addition, by taking the dynamic stiffness values related to the first four modes as the key indexes, Table **1** gives the vibration suppression contribution of such a coating material when it is sprayed on the surface of the composite plate. Note that these dynamic stiffness results are extracted from the trough points in the theoretical and measured curves. According to the deviation results in Table **1**, one can clearly see that when the damping coating is applied, the dynamic stiffness values with different mode rise by 10.9 to 74.7%, which confirms that damping coating does indeed improve the anti-vibration performance of the composite plate. However, the damping effect is closely related to the mode order of the structure as well as the selected boundary condition [28].

4. CONCLUSIONS

In this work, the vibration suppression of composite plates with damping coating is investigated based on a dynamic model developed. Experimental verification is then conducted to prove the effectiveness of such a

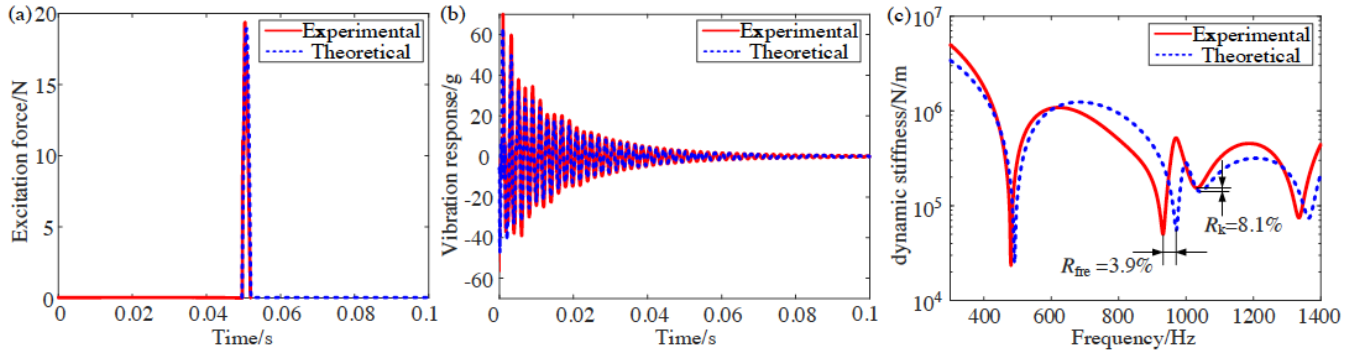

Figure 3: Vibration parameters of the uncoated specimen obtained via experimental tests and theoretical calculations: (**a**) time history of excitation force, (**b**) time history of vibration response, and (**c**) dynamic stiffness curves.

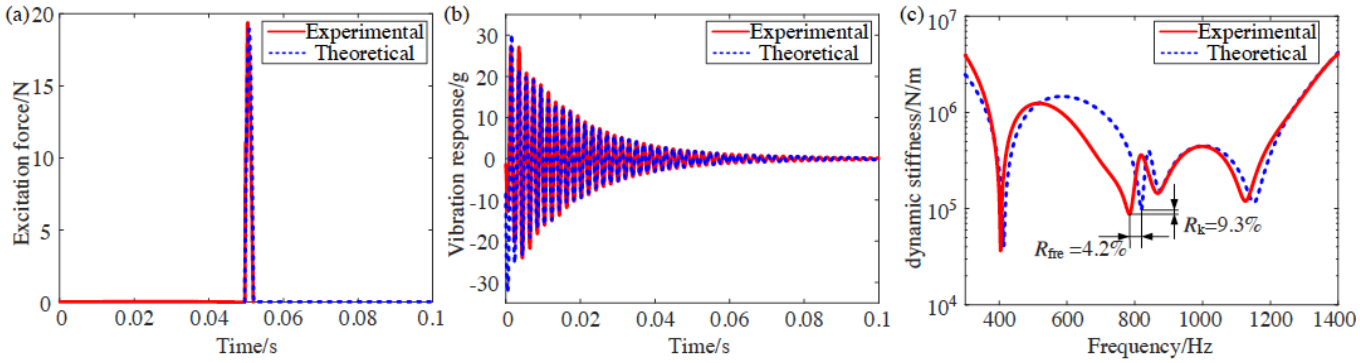

Figure 4: Vibration parameters of the coated specimen obtained via experimental tests and theoretical calculations: (**a**) time history of excitation force, (**b**) time history of vibration response, and (**c**) dynamic stiffness curves.

Table 1: Dynamic Stiffness Value of the Composite Plate Structures with and Without Damping Coating

Type	Dynamic stiffness /N·m^{-1}			
	The 1st Mode	The 2nd Mode	The 3rd Mode	The 4th Mode
Uncoated plate (*A*)	2.463×10^4	5.526×10^4	1.409×10^5	7.393×10^4
Coated plate (*B*)	4.048×10^4	9.653×10^4	1.563×10^5	1.152×10^5
Relative deviation ((*B*-*A*)/*A*) /%	64.4	74.7	10.9	55.8

model. Based on the calculated and experimental results, the following findings are highlighted:

(1) There is a relatively good agreement between the predicted and measured natural frequencies and dynamic stiffness values. Thus, the proposed dynamic model is trustworthy for predicting the vibration parameters.

(2) The damping coating can contribute to the anti-vibration performance of composite plate structure undoubtedly, but the damping effect is closely related to the mode order of such a structure as well as the selected boundary condition.

(3) This study offers a practical tool for the evaluation of the vibration resistance of composite plates coated with DC material, which can be easily extended to the dynamic assessment and analysis of other coated composite structures after the related theoretical model is updated.

ACKNOWLEDGMENT

This study was supported by the Fundamental Research Funds for the Central Universities of China (Grant No. N2104028).

DECLARATION OF CONFLICTING INTERESTS

The authors declare that they have no known competing financial interests or personal relationships that could have appeared to influence the work reported in this paper.

REFERENCES

[1] Qaddoumi N, Yue L-y, Li W, Zu X-d, Huang Z-x, Gao Z-y, *et al*. Performance of carbon fiber reinforced rubber composite armour against shaped charge jet penetration. MATEC Web of Conferences. 2016; 39. https://doi.org/10.1051/matecconf/20163901012

[2] Hong B, Xian G, Wang Z. Durability study of pultruded carbon fiber reinforced polymer plates subjected to water immersion. Advances in Structural Engineering. 2017; 21: 571-9. https://doi.org/10.1177/1369433217732664

[3] Mustafa SAA, Fathy E, Rizk MS. Fiber-reinforced polymer plates for strengthening web opening in steel I-beams under cyclic loading. Advances in Structural Engineering. 2019; 23: 348-59. https://doi.org/10.1177/1369433219868073

[4] Liesmaki O, Plyusnin A, Kulkova J, Lassila LVJ, Vallittu PK, Moritz N. Biostable glass fibre-reinforced dimethacrylate-based composites as potential candidates for fracture fixation plates in toy-breed dogs: Mechanical testing and finite element analysis. J Mech Behav Biomed Mater. 2019; 96: 172-85. https://doi.org/10.1016/j.jmbbm.2019.04.016

[5] Georgantzinos SK, Giannopoulos GI, Markolefas SI. Vibration Analysis of Carbon Fiber-Graphene-Reinforced Hybrid Polymer Composites Using Finite Element Techniques. Materials (Basel). 2020; 13. https://doi.org/10.3390/ma13194225

[6] Pang Y-Y, Wu G, Su Z-L, He X-Y. Experimental study on the carbon-fiber-reinforced polymer-steel interfaces based on carbon-fiber-reinforced polymer delamination failures and hybrid failures. Advances in Structural Engineering. 2020; 23: 2247-60. https://doi.org/10.1177/1369433220911167

[7] Fürbeth W. Special Issue: Advanced Coatings for Corrosion Protection. Materials. 2020; 13: 3401. https://doi.org/10.3390/ma13153401

[8] Dong Y, Han H, Wang F, Zhang Y, Cheng Z, Shi X, *et al*. A low-cost sustainable coating: Improving passive daytime radiative cooling performance using the spectral band complementarity method. Renewable Energy. 2022; 192: 606-16. https://doi.org/10.1016/j.renene.2022.04.093

[9] Zhang J, Zhu X, Yang X, Zhang W. Transient nonlinear responses of an auxetic honeycomb sandwich plate under impact loads. International Journal of Impact Engineering. 2019; 134. https://doi.org/10.1016/j.ijimpeng.2019.103383

[10] Chen Y, Guo H, Sun M, Lv X. Tensile Mechanical Properties and Dynamic Constitutive Model of Polyurea Elastomer under Different Strain Rates. Polymers (Basel). 2022; 14. https://doi.org/10.3390/polym14173579

[11] Zhang H, Li J, Peng T. Development and Mechanical Performance of a New Kind of Bridge Seismic Isolator for Low Seismic Regions. Shock and Vibration. 2013; 20: 725-35. https://doi.org/10.1155/2013/148907

[12] Akbarzadeh AH, Arian Nik M, Pasini D. Vibration responses and suppression of variable stiffness laminates with optimally steered fibers and magnetostrictive layers. Composites Part B: Engineering. 2016; 91: 315-26. https://doi.org/10.1016/j.compositesb.2016.02.003

[13] He ZC, Xiao X, Li E. Design for structural vibration suppression in laminate acoustic metamaterials. Composites

Part B: Engineering. 2017; 131: 237-52. https://doi.org/10.1016/j.compositesb.2017.07.076

[14] Shivakumar J, Ashok MH, Khadakbhavi V, Pujari S, Nandurkar S. Performance analysis of smart laminated composite plate integrated with distributed AFC material undergoing geometrically nonlinear transient vibrations. IOP Conference Series: Materials Science and Engineering. 2018; 310. https://doi.org/10.1088/1757-899X/310/1/012100

[15] Zu X, Wu H, Lv H, Zheng Y, Li H. An Amplitude- and Temperature-Dependent Vibration Model of Fiber-Reinforced Composite Thin Plates in a Thermal Environment. Materials (Basel). 2020; 13. https://doi.org/10.3390/ma13071590

[16] Navaneeth IM, Poojary S, Chandrashekar A, Razak A, Hasan N, Almohana AI, *et al*. Damped Free Vibration Analysis of Woven Glass Fiber-Reinforced Epoxy Composite Laminates. Advances in Materials Science and Engineering. 2022; 2022: 1-13. https://doi.org/10.1155/2022/6980996

[17] Mohotti D, Ngo T, Raman SN, Ali M, Mendis P. Plastic deformation of polyurea coated composite aluminium plates subjected to low velocity impact. Materials & Design (1980-2015). 2014; 56: 696-713. https://doi.org/10.1016/j.matdes.2013.11.063

[18] Kulhavy P, Petru M, Syrovatkova M. Possibilities of the Additional Damping of Unidirectional Fiber Composites by Implementation of Viscoelastic Neoprene and Rubber Layers. Shock and Vibration. 2017; 2017: 1-15. https://doi.org/10.1155/2017/4163485

[19] Xu K, Sun W, Yan X. A structural damping identification technique for coatings on blisks based on improved component mode mistuning model. Thin-Walled Structures. 2020; 151. https://doi.org/10.1016/j.tws.2020.106737

[20] Gao J, Gao Y, Yan X, Jiang J, Xu K, Sun W. Damping mistuning effect of the hard-coating-based intentional mistuning techniques on mistuned blisks and its mechanism. Aerospace Science and Technology. 2020; 101: 105848. https://doi.org/10.1016/j.ast.2020.105848

[21] Wang X, Li X, Yu R-P, Ren J-W, Zhang Q-C, Zhao Z-Y, *et al*. Enhanced vibration and damping characteristics of novel corrugated sandwich panels with polyurea-metal laminate face sheets. Composite Structures. 2020; 251. https://doi.org/10.1016/j.compstruct.2020.112591

[22] Wang X, Li X, Yue Z-S, Yu R-P, Zhang Q-C, Du S-F, *et al*. Optimal design of metallic corrugated sandwich panels with polyurea-metal laminate face sheets for simultaneous vibration attenuation and structural stiffness. Composite Structures. 2021; 256. https://doi.org/10.1016/j.compstruct.2020.112994

[23] Zi B, Jiang F, Wu Y, Bai H, Tang Y, Lu C. Analysis and Experimental Research on Vibration Reduction in Ship High-Temperature Pipeline Based on Long Coated Damping Structure. Journal of Marine Science and Engineering. 2021; 9: 838. https://doi.org/10.3390/jmse9080838

[24] Van Long N, Thinh TI, Bich DH, Tu TM. Nonlinear dynamic responses of sandwich-FGM doubly curved shallow shells subjected to underwater explosions using first-order shear deformation theory. Ocean Engineering. 2022; 260. https://doi.org/10.1016/j.oceaneng.2022.111886

[25] Feli S, Karami L, Jafari SS. Analytical modeling of low velocity impact on carbon nanotube-reinforced composite (CNTRC) plates. Mechanics of Advanced Materials and Structures. 2017; 26: 394-406. https://doi.org/10.1080/15376494.2017.1400613

[26] Kobzili L, Aguib S, Chikh N, Djedid T, Meloussi M. Modeling and simulation of the static and vibratory behavior of hybrid composite plate off-axis anisotropic. Composite Structures. 2021; 273. https://doi.org/10.1016/j.compstruct.2021.114297

[27] Kou H, Yuan H. Rub-induced non-linear vibrations of a rotating large deflection plate. International Journal of Non-Linear Mechanics. 2014; 58: 283-94. https://doi.org/10.1016/j.ijnonlinmec.2013.10.005

[28] Pan S, Dai Q, Safaei B, Qin Z, Chu F. Damping characteristics of carbon nanotube reinforced epoxy nanocomposite beams. Thin-Walled Structures. 2021; 166. https://doi.org/10.1016/j.tws.2021.108127

Received on 05-11-2022 Accepted on 06-12-2022 Published on 13-12-2022

DOI: https://doi.org/10.31875/2409-9848.2022.09.8